Chemistry - Methods

Chemistry—Methods
Chemistry Europe
European Chemical Societies Publishing

RESEARCH ARTICLE OPEN ACCESS

A Differential Alkaline Electrolysis Cell to Study Scaling Effects

Lukas Ritz[1,2] | Martin Müller[1] | Anna K. Mechler[1,2,3] | Felix Lohmann-Richters[1]

[1]Institute of Energy Technologies, Electrochemical Process Engineering (IET-4), Forschungszentrum Jülich GmbH, Jülich, Germany | [2]Electrochemical Reaction Engineering (AVT.ERT), RWTH Aachen University, Aachen, Germany | [3]JARA-ENERGY, Jülich, Germany

Correspondence: Anna K. Mechler (a.mechler@fz-juelich.de) | Felix Lohmann-Richters (f.lohmann-richters@fz-juelich.de)

Received: 9 January 2026 | **Revised:** 6 March 2026 | **Accepted:** 11 March 2026

Keywords: alkaline water electrolysis | differential test cell | hydrogen | operating conditions | scale-up

ABSTRACT

Water electrolysis allows the production of green hydrogen, which will play a key role in the future energy system. While research takes place in small laboratory-scale electrolysis cells, the findings shall be applied to large industrial-scale electrolyzer stacks. What conclusions about the behavior of large stacks can be drawn from small lab cell experiments? In this work, the concept of a differential electrolysis cell was developed to answer this question. The novel cell allows control of relevant operating conditions, most importantly the gas content in the electrolyte and the mechanical contact pressure between electrodes and separator, which is hardly possible with existing standard test cells. We demonstrate that both parameters have an important influence on cell performance. The new test cell will allow in-depth investigation of the observed effects. The cell is configured as an alkaline electrolysis cell, but the concept can be transferred to other types of electrochemical cells. This paves the way to understand and possibly predict the overall performance and limitations of a stack and crucial scaling parameters through small-scale laboratory experiments.

1 | Introduction

Water electrolysis offers the opportunity to produce green hydrogen from water and electric energy from renewable sources. The produced hydrogen can be stored and used as an energy carrier or as a climate-neutral raw material for many chemical products. Alkaline water electrolysis is characterized by a long lifetime and relatively inexpensive components [1–3]. Alkaline electrolyzers are used on a large scale today, and in the future, the size of the systems is expected to grow further [4]. Researchers attempt to optimize and improve the components in many laboratories around the world. Testing of different components, materials, geometries or operating conditions in full-scale is almost impossible for research. Instead, tests are realized on a much smaller lab scale. This raises the question of whether and how findings from the lab can be transferred to the large-scale application. Is it even possible to predict the behavior of large electrolyzers, if only the behavior of lab-cells is known?

The aim of the presented research is to develop a novel measurement device, the "Diffcell", which allows for simulating the operating conditions at different locations in a large electrolyzer in the laboratory and also helps to study local effects inside a larger stack.

The performance of electrolysis cells depends on several operating conditions. The classical operating conditions in alkaline water electrolysis are the temperature, the electrolyte concentration (here, KOH concentration), and the fluid pressure. In addition, other parameters are the electrolyte flow rate and the gas content in the fluid. Another influencing factor is the electrode spacing in a conventional cell, or the mechanical contact pressure between electrode and separator in a zero-gap configuration.

All these operating conditions vary across a large cell or stack. Due to heat production, the temperature at the inlet of a stack will not be the same as the outlet temperature [5]. A pressure loss in the flow field will change the fluid pressure depending on the position. Haas et al. [5] showed this by CFD simulation of a

polymer electrolyte membrane (PEM) electrolyzer flow field. The gas content in the electrolyte increases over the length of the flow channels due to the continuous gas production in the form of dissolved gas or macroscopic gas bubbles. This affects the two-phase flow and the size of the gas bubbles. Water is consumed due to the chemical reaction and transported between anode and cathode due to diffusion, electroosmotic drag and flow as well as convection [6, 7]. This leads to different KOH concentrations at different positions. The electrolyte flow rate will not be perfectly homogeneous over the entire area of a large cell, which was also shown by Haas et al. [5]. Due to component tolerances, or deflection of components caused by mechanical stress, the electrolyte gap (in gap cells) or the contact pressure (in zero-gap cells) will not be the same at every position in a stack. Bates et al. [8] simulated the contact pressure distribution inside different cells of a PEM electrolyzer. Due to the deflection of the endplate, it is not possible to reach a homogeneous contact pressure over the entire active cell area or between the different cells [8, 9].

In order to investigate scaling effects due to locally varying operating conditions, it is first necessary to understand the general influence of all these operating conditions. Many studies investigate and model the influence of the classic operating conditions, pressure, temperature, and KOH concentration, whereby these conditions can be investigated relatively independently of the cell design [10–15]. Temperature and concentration influence the ionic conductivity of the electrolyte, usually ranging from 60°C to 80°C and 25–30 wt% KOH [16, 17]. The effect of the operating pressure is investigated in experimental and simulative studies [11, 14, 18, 19]. Also, there are various studies on the optimal electrode spacing ranging from a few millimeters to a zero-gap configuration of the cell [14, 20, 21]. Using a zero-gap setup, the ohmic resistance of the cell can be reduced by 30% compared to a 2 mm gap [21]. In contrast, Haverkort and Rajaei [22] were able to show an improved "small-gap" cell design with a gap width of 0.2 mm. The optimal gap probably depends on the type of electrode used. There is very little literature about the influence of contact pressure in alkaline cells. Ahn et al. [23] state the optimum contact pressure for their cell at about 4.1 MPa. This optimal contact pressure is specific to each cell setup, and here an anion exchange membrane was used instead of a porous separator [23, 24]. In contrast, Xia et al. [25] found the optimum contact pressure in their setup (featuring an anion exchange membrane as well) to be about 0.5 MPa. On the one hand, increasing contact pressure reduces contact resistances between flow field and electrode which improves the cell performance. On the other hand, compressing the porous electrode and gas diffusion layer leads to a poor transport of produced gases. Remaining gas bubbles can cover active sites of the catalyst and decrease cell performance [23]. The last influencing factor is the gas content in the electrolyte. Various publications show that gas bubbles can have a significant influence on the Ohmic resistance and thus on the performance of cells [21, 26, 27]. For gap cells, gas bubbles in the electrolyte gap reduce the cell performance by decreasing the cross-section for the ionic connection between the electrodes. A higher electrolyte flow rate leads to a faster gas bubble removal. Increasing pressure has a similar effect, because at high pressure the gas bubbles are smaller. This effect becomes stronger for high current densities, when more gas is produced [14]. Also, for zero-gap cells, the electrolyte flow rate influences the cell performance, as shown, for example, by Hnat et al. [28]. Gas bubble removal is also an issue for zero-gap cells because stagnant gas bubbles can block parts of the electrodes [29–31]. Rocha et al. [30] compared natural convection and forced electrolyte flow through their zero-gap cell. With natural convection, the cell voltage increased over time, due to bubble entrapment in the porous foam electrode. Above a certain electrolyte flow rate, such a voltage increase did not occur, and the gas bubble removal was effective.

While classic operating conditions can be tested in standard test cells, investigating the influence of the gas content or mechanical contact pressure is difficult. In standard test cells, varying the contact pressure usually requires disassembly of the cell to adjust the gasket thickness or add spacers, which leads to issues with reproducibility. The gas content in the electrolyte usually increases from the inlet to the outlet. Consequently, the measured current density does not refer to a specific gas content. The other operating conditions are also generally unevenly distributed, resulting in an average current density being measured only.

The concept of a differential cell is known from the field of PEM fuel cells. Here, a relatively small fuel cell is fed by a high reactant stoichiometry. The idea is to reach homogeneous operation conditions independent of location. This technique is, for example, used for the benchmarking of cells or to compare different catalysts [32]. In this work, the differential electrolysis cell (short "Diffcell") is used to analyze a small section of a large cell determined by the corresponding operating conditions. Similarly to the differential fuel cell, it is assumed that the operating conditions within the Diffcell remain constant, because the considered section is small compared to the total area.

The Diffcell makes it possible to control the operating conditions similar to specific positions in a stack, as sketched in Figure 1a, and to study their effects and interactions. The adjustable conditions include classic operating conditions, i.e., pressure, temperature, electrolyte concentration, and flow rate, as well as contact pressure or gap width and the gas content in the electrolyte. Measuring the local cell performance under those conditions allows to understand how a large stack will behave at this position and finally predict the overall stack performance only from lab-scale experiments. This paper presents the design of the Diffcell and demonstrates that previously inaccessible parameters (e.g., contact pressure and gas content) can be examined and that these influence cell performance.

2 | Cell Development

In the Diffcell, it should be possible to set all previously mentioned operating conditions, mimicking specific positions inside a large stack (see Figure 1a). Special focus during cell development are conditions that were hard to control with existing tools and test cells: the mechanical contact pressure between electrodes and diaphragm, and the gas content in the electrolyte.

The concept of the differential cell is adapted from the field of fuel cells. Using a high stoichiometry, for example, the electrolyte flow rate, the operating conditions across the active area can be assumed to be constant. Therefore, setting the operating conditions for a specific point in a stack allows us to measure the local performance at that point. The concept of choosing operating conditions of a certain point within a cell or stack is illustrated with

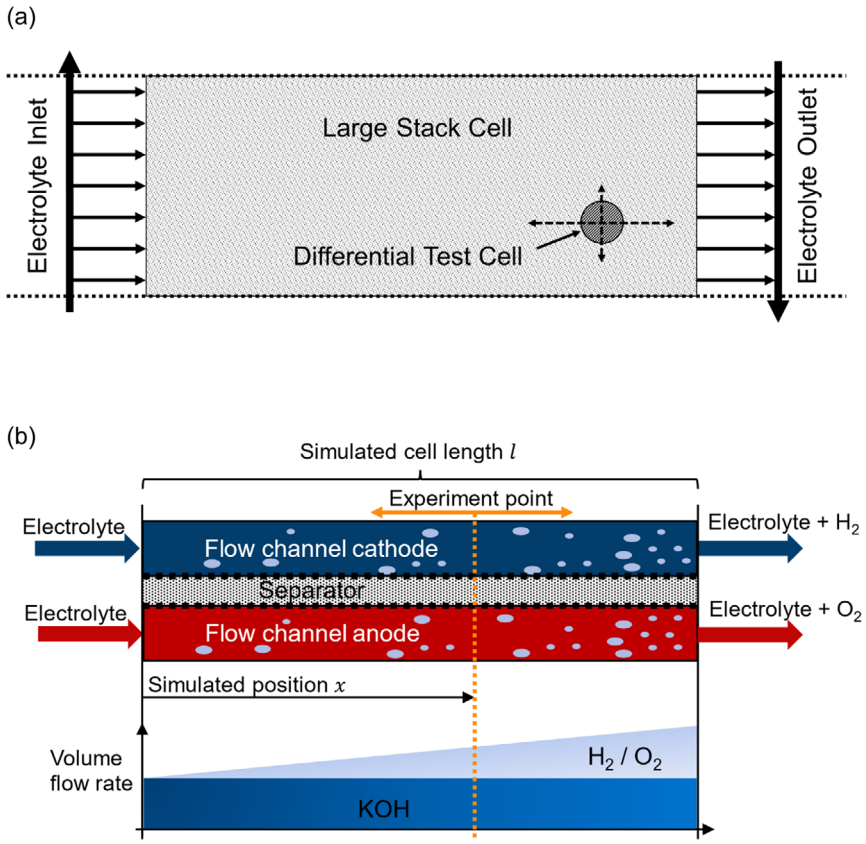

FIGURE 1 | (a) Schematic illustration of the differential test cell as a small section of a large-scale electrolyzer. (b) Illustration of the position of the experiment point depending on electrolyte and gas flow rate.

the gas content as an example in Figure 1b. The amount of gas in the stack increases from the electrolyte inlet to the outlet due to gas production. A specific position defines the experiment point by the electrolyte and gas flow rate, which are supplied to the Diffcell.

The three distinctive features of the Diffcell compared to standard test cells are the adjustability of the contact pressure in the active area only, the possibility of adding gas to the electrolyte prior to the actual electrolysis cell, and the implementation of the differential cell concept.

To vary the contact pressure, the electrode and flow field are movable and can be pressed against the diaphragm and other electrodes from the outside using an adjustment screw.

To supply gas in a similar way to how it would be produced by electrolysis, in front of the actual area to be measured, it is introduced through a porous layer with fine pores, which has a similar structure to electrodes used for electrolysis.

Implementing the differential cell concept involves several measures. On the one hand, the cell area is relatively small, while the flow rate and flow field geometry are designed for a significantly larger active area. Temperature control is located in front of the electrolysis cell to prevent temperature gradients. The advantage of the differential cell over, for example, a segmented cell is that the operating conditions can be freely adjusted to observe the influence of individual parameter changes on current distribution along a channel.

The design of the Diffcell consists of three sections, illustrated in Figure 2a for one half of the cell: (i) the gas feed area, (ii) the inflow length, and (iii) the electrode area. Additionally, a cross-sectional view is shown in Figure 2b. Starting from the electrolyte inlet on the left, the gas is introduced through the gas feed area. This is realized via a porous separating sheet, which enables the precise feed of specific gas contents into the flow channels. The inflow length allows the formation of homogeneous flow conditions toward the electrochemical cell. Finally, the electrode area is located close to the electrolyte outlet. The cell performance resulting from the set conditions is ultimately measured there.

In the following, the general dimensions of the Diffcell are presented, the three sections are described in detail and the features of the cell are summarized. The CAD data for the cell, including assembly drawing and individual drawings for the endplate and flow field stamp, are available in the Forschungszentrum Jülich data repository [33].

The Diffcell has eight parallel flow channels with a cross-section of $4 \times 4\,mm^2$ and an inflow length of 240 mm. The circular electrode area has a diameter of 40 mm, which corresponds to $12.56\,cm^2$. The maximum operating point for the design dimensioning is a simulated active cell area of $200\,cm^2$ (40 mm width and 500 mm length), a current density of $2\,A\,cm^{-2}$ and an electrolyte flow rate of $20\,mL\,cm^{-2}\,min^{-1}$. The cell components are made of pure nickel (>99.2%, material number 2.4068).

2.1 | Gas Feed Area

The Diffcell enables the external supply of gas to simulate the gas production along an electrode in an electrolysis cell. Depending

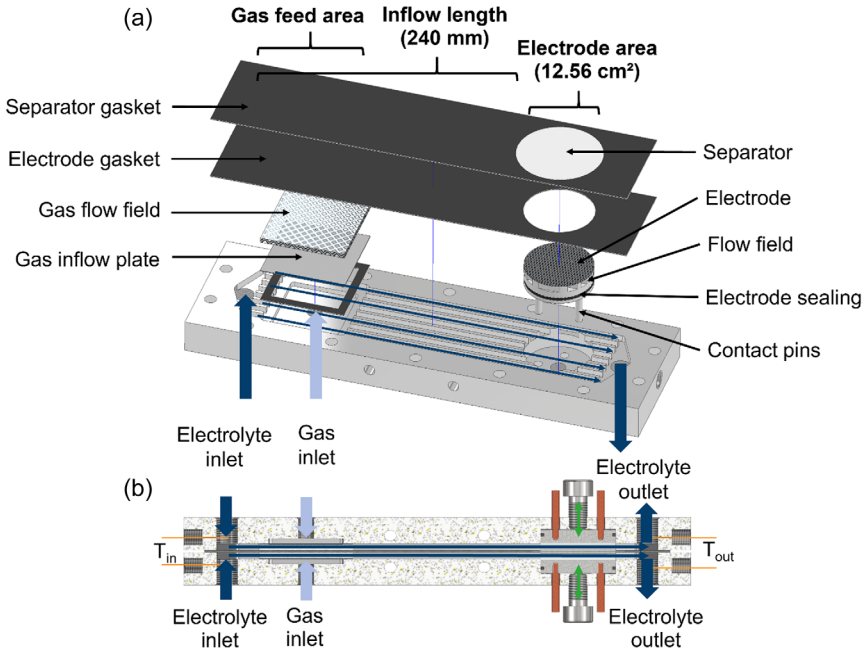

FIGURE 2 | (a) Exploded and (b) sectional view of the Diffcell with labeled components and the three relevant sections. The exploded view only shows one half cell, which is mirrored at the separator. CAD data for the cell are available in the Forschungszentrum Jülich data repository [33].

on the position in the simulated stack, different gas volumes are supplied through the gas feed area. At the inlet of a stack, the gas content is zero, which means no gas is fed to simulate this position. The gas content increases with the cell length, thus a specific position within the stack can be set via the gas volume.

Depending on the position x (experiment point in Figure 1b), the simulated active cell area A_x before this position and the current density i define the gas flow rate $\dot{n}_i$ (H_2 or O_2), present at this point (Equation (1), charge number $z = 2$ for H_2 and $z = 4$ for O_2 and the Faraday constant F). An average current density at the operation point (measured without additional gas) should be used for the calculation. This amount of gas is fed to the Diffcell for the position (x) to be simulated.

$$\text{Gas flow rate } \dot{n}_i = \frac{A_x \cdot i}{z \cdot F} = \frac{x \cdot b \cdot i}{z \cdot F} \tag{1}$$

Adding the highest gas content for the maximum cell size and operating point to be simulated (maximum position x is 500 mm, width of the Diffcell 40 mm, 2 A cm^{-2}), results in 0.124 mol min^{-1} for H_2 und 0.062 mol min^{-1} for O_2 (Equation (2)). For normal conditions, this is 2.79 L min^{-1} H_2 and 1.39 L min^{-1} O_2.

To potentially enable even higher current densities or cell sizes in the future, the maximum gas flow rates for the cell dimensioning are defined to 4 L min^{-1} of H_2 and 2 L min^{-1} of O_2 (including an arbitrary scaling factor of around 1.4).

To imitate the production of gas bubbles on an electrode, the gas is fed through a porous foil. This can be a sheet of sintered metal with fine pores or a porous hydrophobic plastic sheet. The foil should be relatively impermeable to liquid (water or KOH) but permeable to the gas. Here, a titanium sintered foil of 500 µm thickness, 28% porosity, and a mean pore radius of 4 µm was used. The manufacturing process, sintering conditions and more information about the sintered metal foils are given in the publication by Hackemüller et al. [34].

It is important to note that it is an assumption that the introduction of gas through this porous film is similar to gas production at an electrode. Such sintered films are sometimes used as porous transport layers (PTL), especially in PEM and AEM [34–36]. The flow field of the Diffcell in the gas feed area is designed as Ni foam (Recemat BV type Ni-1723.03), which can also be used as a flow field in the active cell area or as the electrode [37].

Alternatively, to investigate the influence of gas in the liquid, the gas could be mixed directly into the tubing in front of the cell, or the concept of a segmented cell could be used [38, 39]. This first option is further from reality than the design used here. The segmented cell has the problem that the influencing factors cannot be easily investigated independently of each other. For example, temperature, gas volume, and current along the cell are related to each other. In addition, the cell length is fixed and therefore less flexible when investigating different cell sizes.

To characterize the film properties of the sintered metal sheet, a defined volume flow of air was passed through a defined area (2 cm^2) of the sintered film and the overpressure was recorded. Figure 3a schematically illustrates the experimental setup. The experiment was carried out once in the dry state of the foil, i.e., without water present in the electrolyte compartment, and once in the flooded state, where the sintered foil retained the water. Figure 3b shows the overpressure for different specific gas flow rates. In the flooded state, a certain overpressure is required to clear the pores of water and allow gas to flow. As the volume flow increases, the overpressure increases linearly. For the flooded case, the slope is three times higher than in the dry state. This preliminary experiment determines the required area of the sintered foil for the design of the gas feed area.

The 25 cm^2 gas feed area in the Diffcell allows for the supply of a sufficient amount of gas at low overpressures using a mass flow controller (MFC). The maximum gas flow of 4 L min^{-1}

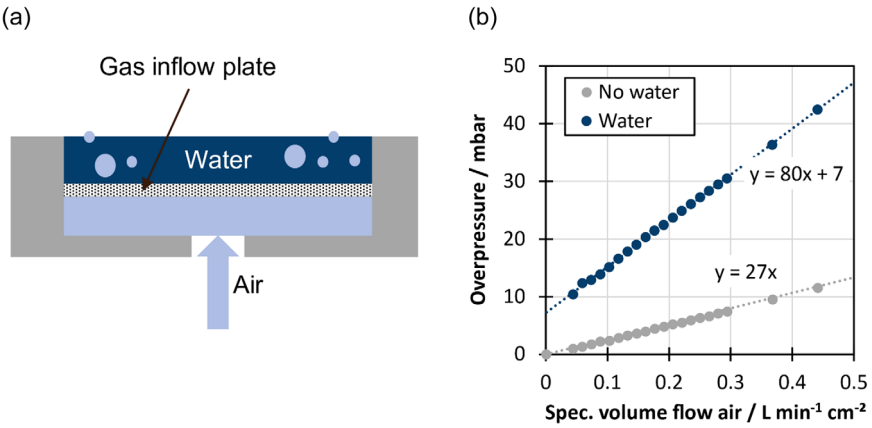

FIGURE 3 | (a) Schematic test setup to measure the pressure drop across the sintered metal foil; (b) measured pressure drop across the sintered metal foil depending on the specific flow rate.

and gas feed area of 25 cm^2 means a specific gas flow of 0.16 L min^{-1} cm^{-2}, so the expected overpressure of about 20 mbar can be read from the chart (blue data points in Figure 3b).

2.2 | Inflow Length

In order to obtain homogeneous flow conditions in front of the electrochemical cell, the Diffcell contains an inflow length with the same channel geometry as the flow field in the electrode area.

When scaling electrolysis cells, the specific volume flow per active area is usually kept constant (mostly in the range of 0.2–20 mL cm^{-2} min^{-1} [11, 30, 37, 40, 41]). In lab cells, usually much higher specific flow rates are used compared to industrial electrolyzers [11, 42, 43]. The electrolyte flow rate $\dot{V}_{KOH}$ for a specific cell length l to be simulated is the multiplication of the simulated length, the width of the Diffcell b (here 40 mm) and the area specific KOH flow rate $\dot{v}_{KOH}$ according to Equation (2) . The calculated amount of electrolyte is fed to the Diffcell, for the cell size (l times b) to be simulated.

Inserting the maximum operating point for the cell dimensions (simulated active cell area 40 mm width and 500 mm length at 20 mL cm^{-2} min^{-1}), Equation (2) yields a KOH flow rate of 4 L min^{-1}. For lower specific flow rates, larger active areas can also be simulated with this electrolyte flow rate.

$$\text{KOH flow rate } \dot{V}_{KOH} = l \cdot b \cdot \dot{v}_{KOH} \tag{2}$$

The required length of the inflow region L_{Hy} can be estimated by Equation (3) for laminar flow using the Reynolds number Re and the hydraulic diameter d_H and for turbulent flow by Equation (4) [44].

The Reynolds number for the gas–liquid mixture is calculated by Equation (5) individually for gas and for liquid from the total flow velocity, assuming plug flow. For the maximum operating point with the total flow rate of 8 L min^{-1} (4 L min^{-1} of KOH plus 4 L min^{-1} of H_2), the flow velocity u in the eight 4×4 mm^2 flow channels is 1.042 m s^{-1}. The hydraulic diameter is 4 mm. At 80°C and 1 bar(a), the dynamic viscosities μ_i of H_2 and KOH (30 wt%) are 9.98 µPa s and 0.9295 mPa s and the respective densities ρ_i are 0.069 and 1258 kg m^{-3} [45, 46]. The calculated Reynolds numbers are 29 (H_2) and 5639 (KOH).

For the turbulent flow, the length of the inflow region is calculated to 240 mm. This length is included in the Diffcell between the electrolyte inlet and the active area, including the gas feed area. An even longer inflow area behind the gas feed area would be advantageous, but it would impair the handling of the cell.

$$\text{Inflow length (laminar)} \quad L_{Hy,l} = 0.03\ Re \cdot d_H \tag{3}$$

$$\text{Inflow length(turbulent)} \quad L_{Hy,t} = 60 \cdot d_H \tag{4}$$

$$\text{Reynolds number} \quad Re_i = \frac{u \cdot \rho_i \cdot d_H}{\mu_i} \tag{5}$$

In order to qualitatively assess the distribution of liquid and gas between the eight flow channels, we conducted an additional experiment in which we mounted half of the Diffcell with a Plexiglas cover and set different flow rates for water and air. Moving gas bubbles were observed in all channels, indicating similar flow rates. A photo from this experiment can be found in Figure S3.

2.3 | Electrode Area

The electrochemical reactions are restricted to the active electrode area. For anode and cathode, the electrode unit consists of a stamp connected to the power supply via contact pins and is sealed with an O-ring (Figure 4). Either a flow field is milled into the stamp (Figure 4a) or a different type of flow field is stacked or welded on top of the stamp. Figure 4b shows an example of a porous nickel-foam utilized as flow field. The electrode is either placed on top of the flow field or is welded to it. The milled flow field has the same channel geometry as the inflow channels. Thus, the flow of the gas–liquid mixture through the cell will not be disturbed.

As shown by the green arrows in Figure 2b, the cell unit is movable in one direction and can be positioned with adjustment screws from the outside. One full turn of the adjusting screw changes the gap width by 1 mm. The correlation between torque and contact pressure for the zero-gap configuration was calibrated in advance using a pressure-sensitive foil, which is shown in the section “Contact pressure adjustment”. The Diffcell supports an electrode gap up to 4 mm and a contact pressure up to 2 MPa in zero-gap configuration.

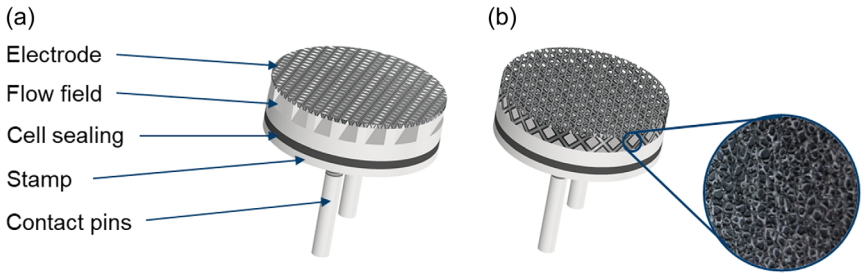

FIGURE 4 | Structure of the electrode unit for a (a) milled flow field and (b) a porous flow field.

2.4 | Features of the Diffcell

This section summarizes how and in which range the operation conditions can be applied in the Diffcell, especially the operating conditions, which cannot be considered with existing test cells. Technical drawings with the geometry details and CAD files of the Diffcell are provided in the Forschungszentrum Jülich data repository [33].

Temperature: As in standard test cells temperature can be varied. By pressurizing the cell, it is possible to reach higher temperatures with the liquid electrolyte. As an additional feature, the temperature of the electrolyte can be measured immediately before and after the cell (yellow lines in Figure 2b). The inflow length is also advantageous for heating the electrolyte to the desired temperature before it reaches the electrode area.

Pressure: Pressurized operation of the differential cell is possible. The presented geometry is mechanically stable for pressurized operation up to 20 bar(g), which was validated by mechanical finite element method (FEM) analysis. The Supporting Information provides further details about the structural mechanical analysis.

KOH-Concentration: The cell is made of pure nickel (>99.2%, material number 2.4068), which has a very good stability against concentrated KOH solution. Nickel is reported to be stable under electrolysis conditions at 40 wt% KOH with oxygen partial pressure from 2 to 18 bar and a temperature of 473 K [47].

KOH Flow-Rate: The Diffcell supports a wide range of electrolyte flow rates. Since the inflow length for turbulent flows is calculated solely from the hydraulic diameter (see Equation (4)), any flow rates can be set in the Diffcell.

Gas Flow-Rate: Due to the size of the gas feed area, it is possible to feed high amounts of gas. Increasing gas content also increases the overpressure at the porous foil. The possibility to feed gas before the cell is one of the most relevant features of the Diffcell. By introducing different amounts of gas to the anode and cathode, co- or counter-flow operation of a cell can be simulated.

Rotation of the Cell: In combination with the injection of gas prior to the active cell area, the orientation of the cell may have a significant influence on the cell performance. Different installation positions in the presence of additional gas in the electrolyte can be investigated with the Diffcell.

Contact Pressure or Gap Width: Via the adjustment screw is possible to change the gap width or the contact pressure during the operation of the cell. The gap can be adjusted from 4 to 0 mm and the contact pressure to the active cell area can be increased up to 2 MPa. In conventional test cells it is necessary to dismount the cell and add spacers to change the gap width or the contact pressure [21]. This usually results in reproducibility issues and a low number of data points. This is overcome using the Diffcell.

Flow Field Type: In the Diffcell it is possible to exchange the type of flow field. Two different flow fields are employed in this work: a milled flow field with the same channel geometry as the inflow area will be used for experiments regarding the gas content in the electrolyte. To investigate the influence of contact pressure, a porous flow field was used to ensure homogeneous contact pressure distribution.

3 | Experimental

The Diffcell as new measurement device offers many advanced possibilities to study the influence of previously inaccessible parameters. The contact pressure adjustment is first validated, before measuring the effect of contact pressure on cell performance and gas crossover. Second, the effect of gas content in the electrolyte on the electrolysis cell is measured with the Diffcell.

3.1 | Contact Pressure Adjustment

Before investigating the influence of the contact pressure on the electrolysis cell, the application of the contact pressure via the adjusting screw was validated. A pressure-sensitive foil from Tekscan (High-speed I-scan, type 5051, measuring range up to 6 MPa) is inserted into the Diffcell, replacing the separator. Figure 5a shows the positioning of the pressure-sensitive film in the Diffcell relative to the electrode area (blue circle) and the adjustment screw (green marking). The contact pressure distribution over the active cell area is measured and visualized for different torques of the adjusting screw.

Apart from replacing the separator with the pressure-sensitive film, the Diffcell was assembled in the same way and with the same components as for the electrochemical measurements. These include the electrode unit, either with foam, or milled flow field and benchmark mesh electrodes from De Nora. A photo of the electrode units is shown in Figure 5b,c.

The torque of the two adjustment screws was gradually increased from 2 to 10 Nm and the force on the electrode area was recorded after 3 min each. After loosening the adjustment screws, this procedure was repeated in a second compression. The contact pressure distribution can be analyzed, as well as the mean contact pressure on the active cell area (marked by the blue circle in Figure 5a).

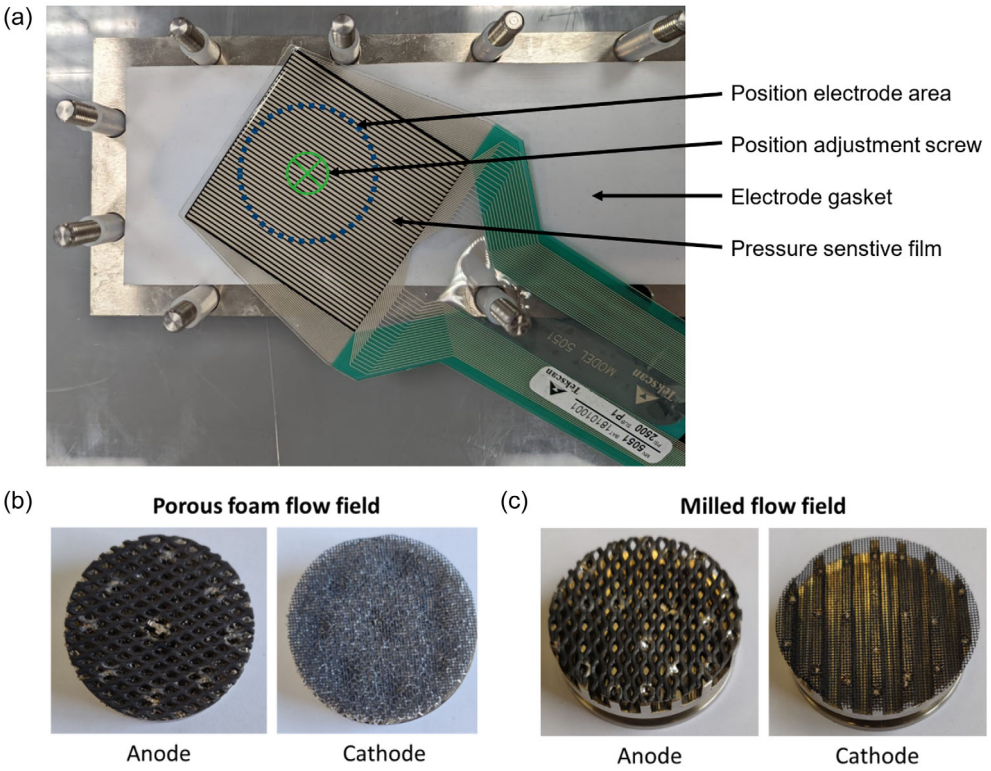

FIGURE 5 | (a) Cell assembly of the Diffcell for contact pressure validation including the pressure sensitive film; (b) electrode unit for anode and cathode with foam flow field and (c) milled flow field.

The influence of the contact pressure on electrochemical cell performance and gas purity (H_2 in O_2) was investigated. The Diffcell is assembled with a Ni foam flow field (Recemat BV type Ni-1116.03) to provide a homogeneous contact pressure on the active cell area. In this study, the porous Ni foam flow field was welded to the stamp. Catalyst-coated mesh electrodes from De Nora (Anode: AENRG® standard, coated on Nickel expanded metal mesh (>98% Ni); Cathode: NRG-R® standard, coated on Nickel woven metal mesh (>98% Ni)) were welded on top of the foam. Figure 5b shows the cell unit including the electrodes. The cell is assembled with a 220 µm thick Zirfon UTP220 separator from AGFA and operated at 80°C and 30 wt% KOH at a flow rate of 100 mL min^{-1}. The experimental setup is illustrated in Figure 6. The Diffcell is shown in the middle and the electrode unit is connected to a BioLogic potentiostat BCS-815. Anolyte and catholyte are fed from the electrolyte tanks by membrane pumps to the Diffcell and removed together with the product gas. The gas/liquid separation takes place in the tanks, which also pre-heat the electrolyte to 80°C. The cell outlet temperature is controlled to 80°C, heated by four heating rods in the inflow length. The oxygen purity in the anode outlet can be analyzed in a gas chromatograph (Micro GC 490 from Agilent Technologies) to detect hydrogen contamination. No gas is added via the gas feed area during the contact pressure experiment.

The electrochemical conditioning of the electrodes was performed before applying any contact pressure in a 1 mm gap configuration. A constant voltage of 2.0 V was applied for 8 h followed by two potentiostatic I–V curves from 1.48 to 2.0 V (3 min per voltage step, mean current density averaged for the last minute). The condition step was repeated. The I–V curves were stable after the second conditioning cycle, meaning that the conditioning period was complete.

By tightening the adjustment screws hand-tight, the electrodes were put in a zero-gap position. The torque of the adjustment screw was then stepwise increased from 2 to 10 Nm. A potentiostatic I–V curve is recorded in each compression step in the same way as during the conditioning. After loosening the adjustment screw, this procedure was repeated as the second compression cycle, starting at 2 Nm. In another two compression cycles the torque was stepwise increased from 2 to 19 Nm.

The product gas purity was measured after the corresponding I–V curve. Therefore, the current density was fixed at 0.05 A cm^{-2} and the H_2 in O_2 content in the anode outlet stream was measured every 2 min with the GC. After 3 h the measurement signal was tending towards a stable final H_2 in O_2 value, which was recorded. In the first compression cycle, gas purity was measured for 1 mm gap, hand-tight adjustment screw, 2, 5, and 10 Nm. In the second compression cycle, it was measured at 2, 5, and 10 Nm, in the third cycle at 15 Nm and finally at 19 Nm in the fourth compression cycle.

3.2 | Gas Content in the Electrolyte

To investigate the influence of gas in the electrolyte, the Diffcell was operated at different gas flow rates and a constant KOH flow rate. As mentioned before, the KOH flow rate defines the simulated cell length which was fixed to 200 mm in this experiment. The gas content increases from the inlet to the outlet and defines the simulated position (see Figure 1b). Via two mass flow controllers (MFC) gas can be applied to the gas feed area of the

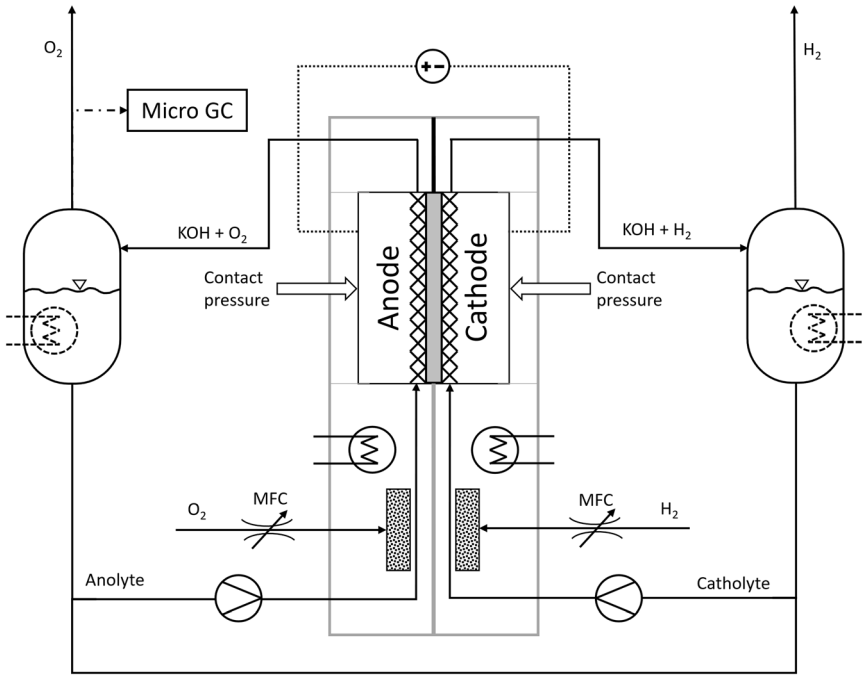

FIGURE 6 | Experimental setup for measuring the influence of contact pressure and gas content in the electrolyte.

Diffcell (Figure 6). Additionally, the cell was rotated to different orientations. The orientation "vertical" means that KOH and gas flow upwards. Horizontal rotation "anode up" and "cathode up" mean horizontal flow with the respective electrode on top. Each of these orientations form an experimental block as shown in Table 1.

For these experiments, the milled flow field and catalyst-coated mesh electrodes (see Figure 5c) were used, Zirfon UTP500 separator, 30 wt% KOH at 80°C and a constant low contact pressure of about 0.2 MPa (2 Nm at the adjustment screw). The electrodes, diaphragm, and cell assembly were reused from a previous experiment on parameter variation of flow rate, temperature, and gas content. The series of experiments presented here aims to measure the relative influence of gas content on the cell rather than to characterize cell components. Reusing the components is intended to provide more stable behavior during the measurement.

The flow rate 480 mL min^{-1} was chosen for a simulated cell length of 200 mm with a specific flow rate of 6 mL cm^{-2} min^{-1}. For the entire experiment the cell voltage was fixed at 2.0 V. The gas flow rates were calculated according to Equation (2) assuming the average current density of 1.1 A cm^{-2} as previously measured at 2.0 V without gas feed. It was calculated for five different positions (0%–100% of the simulated cell length) and added via the MFCs. The operating conditions at the respective positions are summarized in Table 1.

The cell was conditioned at 2.0 V for 14 h and 100 mL min^{-1} KOH flow rate in vertical orientation. Then, the KOH and gas flow rates were set to the previously calculated conditions. At each point, the cell was allowed to stabilize for at least 10 min until the outlet temperature was stable. The mean current density was measured for the next 10 min. After measuring all conditions in vertical orientation, the set was repeated with the anode facing up and the cathode facing up.

The first measurement point in each block (without gas content) was repeated at the end of the block. The standard deviation between those two measurements is used as an estimate of the measurement error for each point within the respective block.

The benchmark points were recorded in the vertical orientation and without gas feed. The current density for each measurement

TABLE 1 | Operating conditions for gas content variation and rotation of the cell.

No.	Simulated cell length, mm	Position	KOH flow, mL min^{-1}	Gas flow cathode, mL min^{-1}	Gas flow anode, mL min^{-1}	Rotation
1	200	0%	480	0	0	Vertical[a]	Anode up	Cathode up
2	200	25%	480	170	85	Vertical	Anode up	Cathode up
3	200	50%	480	340	170	Vertical	Anode up	Cathode up
4	200	75%	480	510	255	Vertical	Anode up	Cathode up
5	200	100%	480	681	340	Vertical	Anode up	Cathode up
6	200	0%	480	0	0	Vertical[a]	Anode up	Cathode up

[a]Benchmark point.

point is expressed as a percentage change relative to the average of the two benchmark points.

4 | Results and Discussion

The results presented in this paper focus on the validation of the Diffcell as well as first results regarding some of the new investigation possibilities. These include the effects of mechanical contact pressure on cell performance and gas crossover, as well as the effect of gas content in the electrolyte channels on cell performance.

4.1 | Influence of Contact Pressure

Figure 7a shows the resulting contact pressure distribution for a milled flow field and a Ni foam flow field at a torque of 10 Nm. A high local contact pressure is represented by red color, while blue means a very low contact pressure. The black color represents areas with a lower contact pressure than the detection limit. The porous structure of the Ni foam as a flow field leads to a more homogeneous contact pressure distribution, while for the milled flow field, the channel-bar structure is clearly visible.

Figure 7b shows the mean contact pressure on the electrode area depending on the torque of the adjustment screw. In all four measurements, the contact pressure increases linearly with the applied torque with roughly the same slope. Hence, it was used as a calibration curve for the proportional relationship between torque and contact pressure.

As previously described, the mechanical compression for the cell performance measurements begins at 1 mm gap configuration. In this configuration, the electrodes were also conditioned as described in the experimental section. Then, the adjustment screw is tightened by hand, followed by four compression cycles in the range of 0.2 MPa (2 Nm) to 2.0 MPa (19 Nm).

Figure 8a shows the I–V curves for selected contact pressures in the first and the fourth compression cycle. The I–V curves for all four compression cycles and all contact pressure steps are given in the Supporting Information (Figure S1). Reducing the gap width from 1 mm to a zero-gap configuration (hand-tight) almost doubles the current density at 2 V. During the initial compression, the current density is further improved with increasing contact pressure. In the fourth compression, the I–V curves are nearly independent of the contact pressure.

The fine cathode mesh initially has a wavy texture, which is a result of the spot welding of the electrode onto the foam flow field (see Figure 5b). Before applying the higher contact pressure for the first time, local gaps may be present, which are compensated by plastic deformation of the foam. This increases the contact area with the diaphragm, eliminates gaps, and consequently improves performance with increasing contact pressure in the first compression cycle. The mechanical compression of the cell, particularly during the initial compression, leads to a plastic deformation of the nickel foam flow field (approx. 35% compression after the four compression cycles). A photo of the electrode unit with the compressed foam flow field is shown in the Supporting Information (Figure S2). The flow field compression probably has a negative influence on the flow distribution and the removal of gas bubbles. This leads to unclear trends within the second compression, which require in-depth investigation which is beyond the scope of this work. From the third compression of the cell, almost no further plastic deformation of the Ni foam takes place, resulting in reproducible and contact-pressure-independent polarization curves. The welding of the electrodes to the flow field eliminates pressure-dependent contact resistances.

Comparing a 2 mm gap cell with a zero-gap configuration, Phillips et al. [21] also measured an improved cell performance, which was explained by a decrease in the Ohmic resistance.

There is no literature in the field of alkaline electrolysis on the influence of contact pressure on cell performance, so the results can only be compared with those of PEM and AEM electrolysis. There, a considerable influence of contact pressure on cell performance is described [23, 25, 48–50]. The optimum contact pressure depends on the individual cell set-up and is given by Ahn [23] as 4.1 MPa or by Xia [25] as 0.5 MPa. Both use an

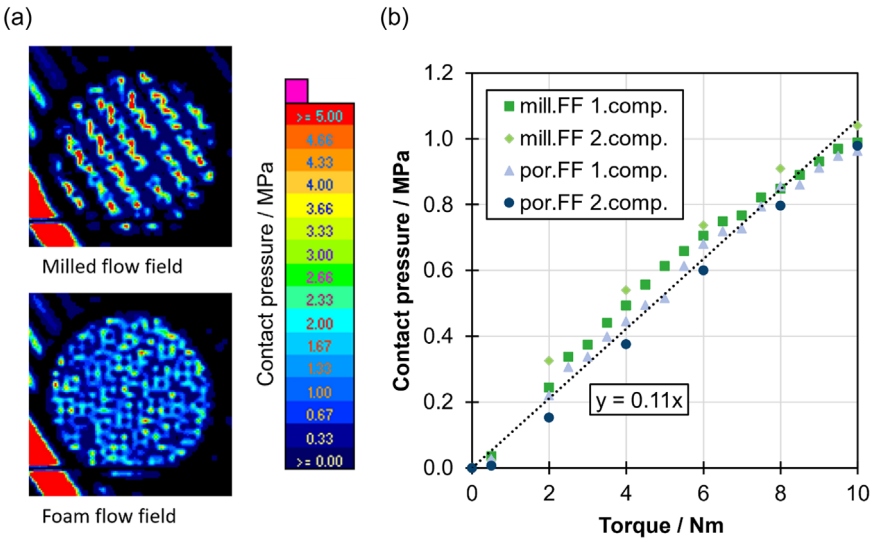

FIGURE 7 | (a) Measurement of the contact pressure with the pressure-sensitive foil for milled and Ni foam flow field (10 Nm, first compression). (b) Mean contact pressure depending on the torque of the adjusting screw.

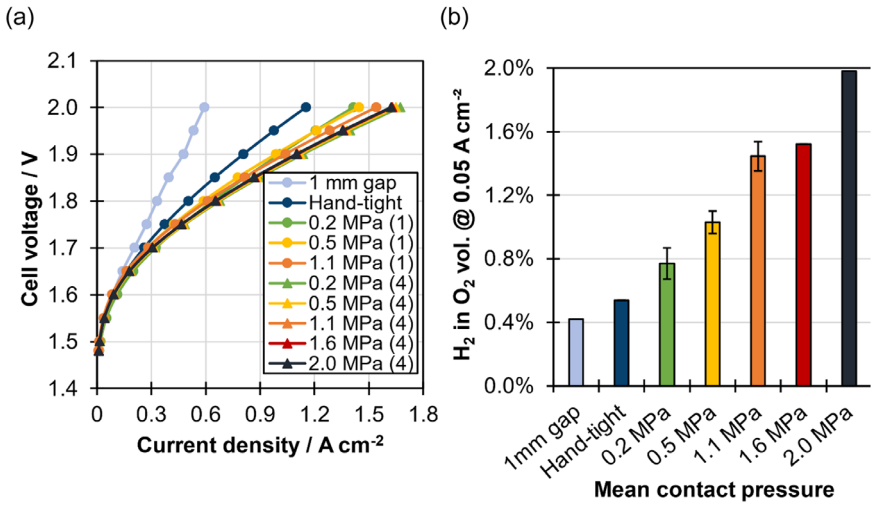

FIGURE 8 | (a) I–V curves for selected contact pressures in compression cycle 1 and 4 at 80°C, 30 wt% KOH, 100 mL min^{-1}; (b) H_2 in O_2 gas contamination for different contact pressures at 0.05 A cm^{-2}. For 0.2, 0.5, and 1.1 MPa two data points for the gas cross over were recorded, the error bars represent the standard deviation. The data points for 1 mm gap, hand-tight, 1.6, and 2.0 MPa are single determinations.

ion-conducting membrane instead of a porous separator in their cell. Decreasing contact resistances with increasing contact pressure are given as one of the main reasons for the performance variation. Since the electrodes are welded to the flow field in the Diffcell, there are no contact resistances that depend on the contact pressure, explaining the minor influence of the compression on the cell performance from the third compression cycle of the cell.

Figure 8b shows the measured gas purity (H_2 in O_2) for different contact pressures at low current density (0.05 A cm^{-2}). Assuming a full zero-gap configuration of the cell at 0.2 MPa, the gas crossover is twice that of the 1 mm gap configuration. A further increase in contact pressure leads to even higher crossover values. At 2 MPa, the contamination level reaches almost 2%, which is the upper limit for safe operation. While no reports about the influence of contact pressure on gas quality in alkaline electrolysis could be found at the time of this study, the impact of gap size was evaluated regarding the crossover in small-gap cells. The cathodic gap was found as an important parameter for hydrogen crossover [51]. A zero-gap configuration massively increased the crossover (approx. factor 10) compared to a 500 µm small-gap cell, both using the UTP220 diaphragm [51].

An increasing hydrogen crossover with increasing contact pressure is also reported for polymer electrolyte membrane electrolyzers [49, 50, 52]. It is assumed that mechanical stress on the membrane causes it to become thinner at certain spots, resulting in an inhomogeneous current density distribution and increased crossover.

An in-depth study is needed to improve the understanding of this effect and its dependence on the cell components, like the flow field and electrode, especially for alkaline water electrolysis.

4.2 | Influence of Gas Content in the Electrolyte

To validate the possibility of modeling different positions in a larger cell, the impact of varying gas content on the cell performance was investigated. Figure 9a illustrates how different positions along a larger cell can be simulated by adding increasing amounts of gas to the electrolyte stream. Furthermore, the influence of cell orientation, i.e., vertical or horizontal with either anode or cathode on top, was investigated.

Without gas feed, the current densities at 2 V were 0.907 A cm^{-2} in vertical orientation, 0.910 A cm^{-2} in anode up orientation, and 0.848 A cm^{-2} in cathode up orientation. Including the gas content, the obtained current densities at 2 V are shown relative to the benchmark configuration (vertical, no gas feed) in Figure 9b. The supply of gas to the electrolyte, respectively, a position closer to the outlet of the simulated cell, increases the current density relative to the benchmark (without gas feed). The vertical orientation (blue) and horizontal orientation with the anode on top (up) (green) deliver higher current densities compared to the cathode up configuration (orange).

The influence of cell orientation on current density might be due to the different structure of anode and cathode electrodes, featuring a larger mesh size of the anode. In the cathode up orientation, the anode is at the bottom. We assume that the larger mesh size of the anode (see Figure 5c) probably tends to trap gas bubbles rising into the electrode pores, consequently blocking parts of the electrode. Haverkort et al. [31] and Rocha et al. [30] found that the size of the electrode holes is an important parameter for trapping bubbles. If this is also the case here and how this is affected by the electrode orientation is subject to further investigation.

Overall, adding gas into the electrolyte stream improves the current density in all experiments by up to 4%. We hypothesize that the added gas improves the removal of gas bubbles, which block parts of the electrode. This could be due to the increased flow velocity, as well as to coalescence of stagnant bubbles with floating ones. Literature presents stagnant gas bubbles at the electrode as negatively affecting cell performance by blocking parts of the electrode and increasing the length of the current pathway [23, 26, 31]. A sufficient supply of electrolyte is necessary to ensure a utilization of the active cell area and the flooding of the cell [28]. Increased flow rate and flow velocity have been reported to improve the current density, due to better bubble removal [30]. Caution needs to be practiced when comparing

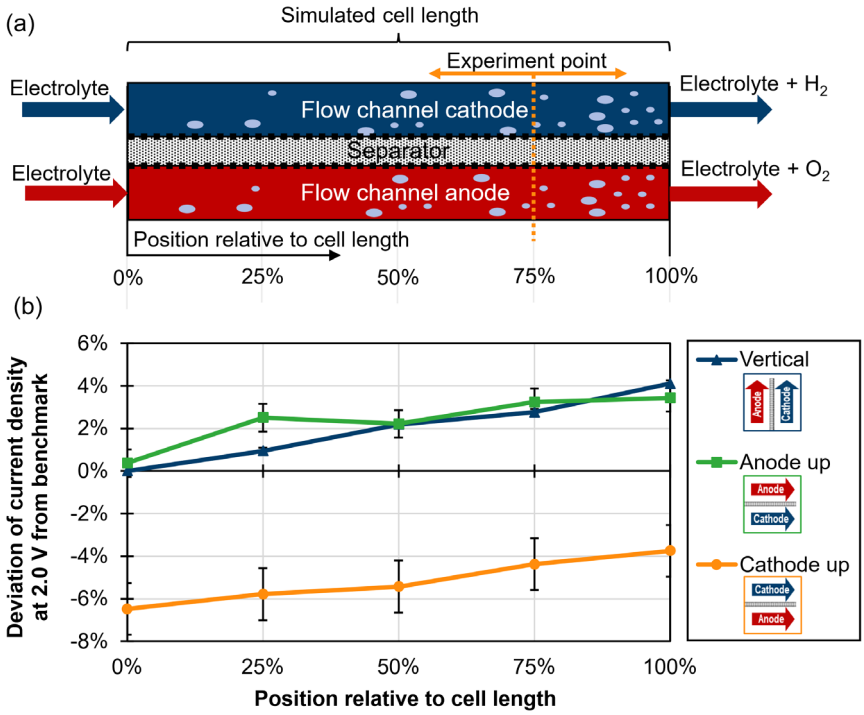

FIGURE 9 | (a) Simulating different positions in a large electrolyzer by the local gas content. The experiment point is defined by the gas content, increasing from the electrolyte inlet the outlet. (b) Deviation of the current density from the benchmark (vertical, no gas) due to the increasing gas content. Operating conditions: 2.0 V, 80°C, 30 wt% KOH, 480 mL min^{-1}.

such effects with gap cells, in which bubbles in the gap increase the ohmic resistance [21, 30]. The observed current increase when adding gas to the electrolyte flow is thus in accordance with previous literature reports. Nevertheless, further investigations are necessary to understand this effect and its dependence on the cell components and other operating parameters in detail.

5 | Conclusion

In this work, we have demonstrated the advantages of the differential alkaline electrolysis cell ("Diffcell"). There are three distinctive features of the Diffcell compared to standard test cells: The adjustability of the contact pressure in the active area only, the possibility of adding gas to the electrolyte prior to the actual electrolysis cell, and the implementation of the differential cell concept.

Contact pressure measurements show that the Diffcell allows to independently adjust the contact pressure to the active cell area. Measurements of cell performance for different contact pressures and cycles reveal an improvement in current density with increasing pressure during the first compression. After several contact pressure cycles, the current density is independent of the pressure. Interestingly, a higher contact pressure has a negative effect on the H_2 crossover.

Increasing the gas content in the electrolyte mimics the local operating conditions at various positions across a cell or stack. Our results indicate that higher gas contents might actually improve the local performance due to higher flow velocities and hence bubble removal along the electrode.

In summary, our results show the importance of contact pressure and gas content on the electrochemical performance. The Diffcell enables in-depth future studies into the effect of these parameters in combination with different components and electrode configurations, as the observed effects certainly depend on the specific cell components.

Combining measurements of the novel cell with a stack that has a known distribution of local operating conditions will be the next step toward understanding and predicting scaling effects. This could validate the general concept at the target scale. Additional scaling effects, such as shunt currents, will require different tools.

The concept is demonstrated for alkaline electrolysis in this work, but can be readily transferred to other electrochemical reactors. Future investigations using this novel cell design will foster an understanding of scale-up effects and crucial parameters in stack design. The simple yet effective cell design enables systematic studies with minimized experimental effort. This is an important step towards fast and efficient scaling from single cells in the laboratory to industrially relevant stack sizes.

Acknowledgments

The presented research is funded by the German Federal Ministry of Economic Affairs and Energy in the project "NextH_2 - Next generation of powerful and efficient alkaline electrolyzers for regenerative H2 generation" (Reference 03EI3011A-C) and by the Deutsche Forschungsgemeinschaft (DFG, German Research Foundation)—491111487. The authors thank the project partners Agfa, thyssenkrupp nucera, and De Nora for their valuable contributions. In addition, the authors would like to express their gratitude to all IET-4 colleagues involved, with particular acknowledgement to Norbert Commerscheidt and Walter Zwaygardt for their assistance with the experimental setup.

Open Access funding enabled and organized by Projekt DEAL.

Funding

This work was supported by Bundesministerium für Wirtschaft und Energie (03EI3011A-C) and Deutsche Forschungsgemeinschaft (491111487).

Data Availability Statement

The data that support the findings of this study are openly available in Jülich DATA at https://doi.org/10.26165/JUELICH-DATA/BLENZY, reference number 33.

References

1. J. C. Ehlers, A. A. Feidenhans'l, K. T. Therkildsen, and G. O. Larrazábal, "Affordable Green Hydrogen from Alkaline Water Electrolysis: Key Research Needs from an Industrial Perspective," *ACS Energy Letters* 8 (2023): 1502, https://doi.org/10.1021/acsenergylett.2c02897.

2. S. E. Hosseini and M. A. Wahid, "Hydrogen Production from Renewable and Sustainable Energy Resources: Promising Green Energy Carrier for Clean Development," *Renewable and Sustainable Energy Reviews* 57 (2016): 850, https://doi.org/10.1016/j.rser.2015.12.112.

3. I. Dincer and C. Acar, "Review and Evaluation of Hydrogen Production Methods for Better Sustainability," *International Journal of Hydrogen Energy* 40 (2015): 11094, https://doi.org/10.1016/j.ijhydene.2014.12.035.

4. C. Karacan, F. P. Lohmann-Richters, G. P. Keeley, et al., "Challenges and Important Considerations when Benchmarking Single-Cell Alkaline Electrolyzers," *International Journal of Hydrogen Energy* 47 (2022): 4294–4303, https://doi.org/10.1016/j.ijhydene.2021.11.068.

5. C. Haas, M.-G. Macherhammer, N. Klopcic, and A. Trattner, "Capabilities and Limitations of 3D-CFD Simulation of Anode Flow Fields of High-Pressure PEM Water Electrolysis," *Processes* 9 (2021): 968, https://doi.org/10.3390/pr9060968.

6. J. W. Haverkort, "Modeling and Experiments of Binary Electrolytes in the Presence of Diffusion, Migration, and Electro-Osmotic Flow," *Physical Review Applied* 14 (2020): 044047, https://doi.org/10.1103/PhysRevApplied.14.044047.

7. J. W. Haverkort and H. Rajaei, "Electro-Osmotic Flow and the Limiting Current in Alkaline Water Electrolysis," *Journal of Power Sources Advances* 6 (2020): 100034, https://doi.org/10.1016/j.powera.2020.100034.

8. A. Bates, S. Mukherjee, S. Hwang, et al., "Simulation and Experimental Analysis of the Clamping Pressure Distribution in a PEM Fuel Cell Stack," *International Journal of Hydrogen Energy* 38 (2013): 6481.

9. M. Jo, H.-S. Cho, and Y. Na, "Comparative Analysis of Circular and Square End Plates for a Highly Pressurized Proton Exchange Membrane Water Electrolysis Stack," *Applied Sciences* 10 (2020): 6315, https://doi.org/10.3390/app10186315.

10. D. Jang, W. Choi, H.-S. Cho, C. C. Won, C. H. Kim, and S. Kang, "Numerical Modeling and Analysis of the Temperature Effect on the Performance of an Alkaline Water Electrolysis System," *Journal of Power Sources* 506 (2021): 230106, https://doi.org/10.1016/j.jpowsour.2021.230106.

11. M. T. de Groot, J. Kraakman, and R. L. Garcia Barros, "Optimal Operating Parameters for Advanced Alkaline Water Electrolysis," *International Journal of Hydrogen Energy* 47 (2022): 34773, https://doi.org/10.1016/j.ijhydene.2022.08.075.

12. T. Adibi, A. Sojoudi, and S. C. Saha, "Modeling of Thermal Performance of a Commercial Alkaline Electrolyzer Supplied with Various Electrical Currents," *International Journal of Thermofluids* 13 (2022): 100126, https://doi.org/10.1016/j.ijft.2021.100126.

13. C. Henao, K. Agbossou, M. Hammoudi, Y. Dubé, and A. Cardenas, "Simulation Tool Based on a Physics Model and an Electrical Analogy for an Alkaline Electrolyser," *Journal of Power Sources* 250 (2014): 58, https://doi.org/10.1016/j.jpowsour.2013.10.086.

14. D. Jang, H.-S. Cho, and S. Kang, "Numerical Modeling and Analysis of the Effect of Pressure on the Performance of an Alkaline Water Electrolysis System," *Applied Energy* 287 (2021): 116554, https://doi.org/10.1016/j.apenergy.2021.116554.

15. E. Amores, J. Rodriguez, and C. Carreras, "Influence of Operation Parameters in the Modeling of Alkaline Water Electrolyzers for Hydrogen Production," *International Journal of Hydrogen Energy* 39 (2014): 13063, https://doi.org/10.1016/j.ijhydene.2014.07.001.

16. R. Bhandari, C. A. Trudewind, and P. Zapp, "Life Cycle Assessment of Hydrogen Production via Electrolysis—A Review," *Journal of Cleaner Production* 85 (2014): 151, https://doi.org/10.1016/j.jclepro.2013.07.048.

17. D. M. See and R. E. White, "Temperature and Concentration Dependence of the Specific Conductivity of Concentrated Solutions of Potassium Hydroxide," *Journal of Chemical & Engineering Data* 42 (1997): 1266.

18. J. Brauns and T. Turek, "Model-Based Analysis and Optimization of Pressurized Alkaline Water Electrolysis Powered by Renewable Energy," *Journal of the Electrochemical Society* 170 (2023): 064510, https://doi.org/10.1149/1945-7111/acd9f1.

19. Y. Li, T. Zhang, J. Ma, et al., "Study the Effect of Lye Flow Rate, Temperature, System Pressure and Different Current Density on Energy Consumption in Catalyst Test and 500W Commercial Alkaline Water Electrolysis," *Materials Today Physics* 22 (2022): 100606, https://doi.org/10.1016/j.mtphys.2022.100606.

20. N. Nagai, M. Takeuchi, T. Kimura, and T. Oka, "Existence of Optimum Space between Electrodes on Hydrogen Production by Water Electrolysis," *International Journal of Hydrogen Energy* 28 (2003): 35, https://doi.org/10.1016/S0360-3199(02)00027-7.

21. R. Phillips, A. Edwards, B. Rome, D. R. Jones, and C. W. Dunnill, "Minimising the Ohmic Resistance of an Alkaline Electrolysis Cell through Effective Cell Design," *International Journal of Hydrogen Energy* 42 (2017): 23986–23994, https://doi.org/10.1016/j.ijhydene.2017.07.184.

22. J. W. Haverkort and H. Rajaei, "Voltage Losses in Zero-Gap Alkaline Water Electrolysis," *Journal of Power Sources* 497 (2021): 229864, https://doi.org/10.1016/j.jpowsour.2021.229864.

23. S. H. Ahn, B.-S. Lee, I. Choi, et al., "Development of a Membrane Electrode Assembly for Alkaline Water Electrolysis by Direct Electrodeposition of Nickel on Carbon Papers," *Applied Catalysis B: Environmental* 154-155 (2014): 197, https://doi.org/10.1016/j.apcatb.2014.02.021.

24. R. Phillips and C. W. Dunnill, "Zero Gap Alkaline Electrolysis Cell Design for Renewable Energy Storage as Hydrogen Gas," *RSC Advances* 6 (2016): 100643–100651, https://doi.org/10.1039/c6ra22242k.

25. L. Xia, S. Holtwerth, C. Rodenbücher, W. Lehnert, M. Shviro, and M. Müller, "Effects of Mechanical Pressure on Anion Exchange Membrane Water Electrolysis: A Non-Negligible yet Neglected Factor," *Journal of Power Sources* 590 (2024): 233802, https://doi.org/10.1016/j.jpowsour.2023.233802.

26. H. Vogt, "The Actual Current Density of Gas-Evolving Electrodes—Notes on the Bubble Coverage," *Electrochimica Acta* 78 (2012): 183, https://doi.org/10.1016/j.electacta.2012.05.124.

27. R. Iwata, L. Zhang, K. L. Wilke, et al., "Bubble Growth and Departure Modes on Wettable/Non-Wettable Porous Foams in Alkaline Water Splitting," *Joule* 5 (2021): 887, https://doi.org/10.1016/j.joule.2021.02.015.

28. J. Hnat, R. Kodym, K. Denk, M. Paidar, J. Zitka, and K. Bouzek, "Design of a Zero-Gap Laboratory-Scale Polymer Electrolyte Membrane Alkaline Water Electrolysis Stack," *Chemie Ingenieur Technik* 91 (2019): 821, https://doi.org/10.1002/cite.201800185.

29. H. Vogt, "The Quantities Affecting the Bubble Coverage of Gas-Evolving Electrodes," *Electrochimica Acta* 235 (2017): 495, https://doi.org/10.1016/j.electacta.2017.03.116.

30. F. Rocha, R. Delmelle, C. Georgiadis, and J. Proost, "Effect of Pore Size and Electrolyte Flow Rate on the Bubble Removal Efficiency of 3D Pure Ni Foam Electrodes during Alkaline Water Electrolysis," *Journal of Environmental Chemical Engineering* 10 (2022): 107648, https://doi.org/10.1016/j.jece.2022.107648.

31. J. W. Haverkort, A. S. Aghdam, and E. J. B. Craye, "The Optimal Electrode Hole Size in Zero Gap Alkaline Water Electrolysis: A Combined Electrochemical, Theoretical, and Bubble Imaging Approach," *International Journal of Hydrogen Energy* 171 (2025): 150919, https://doi.org/10.1016/j.ijhydene.2025.150919.

32. R. Riasse, C. Lafforgue, F. Vandenberghe, et al., "Benchmarking Proton Exchange Membrane Fuel Cell Cathode Catalyst at High Current Density: A Comparison between the Rotating Disk Electrode, the Gas Diffusion Electrode and Differential Cell," *Journal of Power Sources* 556 (2023): 232491, https://doi.org/10.1016/j.jpowsour.2022.232491.

33. L. Ritz, M. Müller, A. K. Mechler, and F. Lohmann-Richters, *A Differential Alkaline Electrolysis Cell to Study Scaling Effects* (Jülich DATA, 2026), https://doi.org/10.26165/JUELICH-DATA/BLENZY.

34. F. J. Hackemüller, E. Borgardt, O. Panchenko, M. Müller, and M. Bram, "Manufacturing of Large-Scale Titanium-Based Porous Transport Layers for Polymer Electrolyte Membrane Electrolysis by Tape Casting," *Advanced Engineering Materials* 21 (2019): 1801201, https://doi.org/10.1002/adem.201801201.

35. E. Borgardt, O. Panchenko, F. J. Hackemüller, et al., "Mechanical Characterization and Durability of Sintered Porous Transport Layers for Polymer Electrolyte Membrane Electrolysis," *Journal of Power Sources* 374 (2018): 84, https://doi.org/10.1016/j.jpowsour.2017.11.027.

36. N. U. Hassan, E. Motyka, J. Kweder, et al., "Effect of Porous Transport Layer Properties on the Anode Electrode in Anion Exchange Membrane Electrolyzers," *Journal of Power Sources* 555 (2023): 232371, https://doi.org/10.1016/j.jpowsour.2022.232371.

37. S. Appelhaus, L. Ritz, S.-V. Pape, et al., "Benchmarking Performance: A Round-Robin Testing for Liquid Alkaline Electrolysis," *International Journal of Hydrogen Energy*. (2024): 1004–1010, https://doi.org/10.1016/j.ijhydene.2024.11.288.

38. N. Hensle, S. Metz, A. Weber, and T. Smolinka, "A Segmented Along the Channel Test Cell for Locally Resolved Analysis at High Current Densities in PEM Water Electrolysis," *Journal of the Electrochemical Society* 171 (2024): 114510, https://doi.org/10.1149/1945-7111/ad9064.

39. I. Biswas, D. G. Sánchez, M. Schulze, et al., "Advancement of Segmented Cell Technology in Low Temperature Hydrogen Technologies," *Energies* 13 (2020): 2301, https://doi.org/10.3390/en13092301.

40. S. Renz, T. Arlt, N. Kardjilov, et al., "Operando Investigation of the Two-Phase Flow Behavior of a Zero-Gap Alkaline Electrolysis Cell Using Neutron Radiography," *International Journal of Hydrogen Energy* 157 (2025): 150321, https://doi.org/10.1016/j.ijhydene.2025.150321.

41. S. Abdelghani-Idrissi, N. Dubouis, A. Grimaud, P. Stevens, G. Toussaint, and A. Colin, "Effect of Electrolyte Flow on a Gas Evolution Electrode," *Scientific Reports* 11 (2021): 4677, https://doi.org/10.1038/s41598-021-84084-1.

42. P. Trinke, P. Haug, J. Brauns, B. Bensmann, R. Hanke-Rauschenbach, and T. Turek, "Hydrogen Crossover in PEM and Alkaline Water Electrolysis. Mechanisms, Direct Comparison and Mitigation Strategies," *Journal of the Electrochemical Society* 165 (2018): F502–F513, https://doi.org/10.1149/2.0541807jes.

43. P. Haug, M. Koj, and T. Turek, "Influence of Process Conditions on Gas Purity in Alkaline Water Electrolysis," *International Journal of Hydrogen Energy* 42 (2017): 9406–9418, https://doi.org/10.1016/j.ijhydene.2016.12.111.

44. L. Prandtl, K. Oswatitsch, and K. Wieghardt, *Führer Durch Die Strömungslehre* (Vieweg, 2020).

45. VDI Heat Atlas, *VDI Heat Atlas* (Springer, 2010).

46. A. Hodges, S. Renz, F. Lohmann-Richters, et al., "Critical Analysis of Published Physical Property Data for Aqueous Potassium Hydroxide. Collation into Detailed Models for Alkaline Electrolysis," *Journal of Chemical and Engineering Data* 68 (2023): 1485, https://doi.org/10.1021/acs.jced.3c00040.

47. P. Drodten and D. Schedlitzki, "Potassium Hydroxide", in *Corrosion Handbook. Corrosive Agents and Their Interaction with Materials*, ed. G. Kreysa and M. Schütze (Wiley-VCH, 2007), 1–237.

48. S. Al Shakhshir, X. Cui, S. Frensch, and S. K. Kær, "In-Situ Experimental Characterization of the Clamping Pressure Effects on Low Temperature Polymer Electrolyte Membrane Electrolysis," *International Journal of Hydrogen Energy* 42 (2017): 21597–21606, https://doi.org/10.1016/j.ijhydene.2017.07.059.

49. A. Martin, P. Trinke, M. Stähler, et al., "The Effect of Cell Compression and Cathode Pressure on Hydrogen Crossover in PEM Water Electrolysis," *Journal of the Electrochemical Society* 169 (2022): 014502, https://doi.org/10.1149/1945-7111/ac4459.

50. M. Stähler, A. Stähler, F. Scheepers, M. Carmo, W. Lehnert, and D. Stolten, "Impact of Porous Transport Layer Compression on Hydrogen Permeation in PEM Water Electrolysis," *International Journal of Hydrogen Energy* 45 (2020): 4008–4014, https://doi.org/10.1016/j.ijhydene.2019.12.016.

51. R. Lira Garcia Barros, J. T. Kraakman, C. Sebregts, J. van der Schaaf, and M. T. de Groot, "Impact of an Electrode-Diaphragm Gap on Diffusive Hydrogen Crossover in Alkaline Water Electrolysis," *International Journal of Hydrogen Energy* 49 (2024): 886–896, https://doi.org/10.1016/j.ijhydene.2023.09.280.

52. A. Hintzen, M. Stähler, and I. Friedrich, "Membrane Creep Caused by Porous Transport Layer Compression in PEM Water Electrolysis and the Impact on Hydrogen Permeation," *Journal of the Electrochemical Society* 172 (2025): 044512, https://doi.org/10.1149/1945-7111/adcd00.

Supporting Information

Additional supporting information can be found online in the Supporting Information section. Regarding the influence of mechanical contact pressure, it contains I-V-curves for all measured contact pressures and compression cycles **(Supporting Fig. S1)**, as well as a photo of the electrode stamp after compression **(Supporting Fig. S2)**. Regarding the effect of gas bubbles in the electrolyte, an additional experiment was conducted to observe the distribution of gas bubbles in the flow channels **(Supporting Fig. S3)**. A FEM simulation verified the mechanical stability of the Diffcell, and the supporting information describes this simulation (**Supporting Fig. S4** to **Supporting Fig. S8** and **Supporting Table S1**).